Darkfield orthogonal polarized spectral imaging for studying endovascular laser-tissue interactions in vivo – a preliminary study

Michal Heger, Johan F. Beek, Karin Stenback, Dirk J. Faber, and Martin J.C. van Gemert

Laser Center, Academic Medical Center, University of Amsterdam, Meibergdreef 9, 1105 AZ Amsterdam, The Netherlands
M.Heger@amc.uva.nl

Can Ince

Department of Physiology, Academic Medical Center, University of Amsterdam, Meibergdreef 9, 1105 AZ Amsterdam, The Netherlands

Abstract: Due to the limited number of suitable intravital microscopy techniques, relatively little is known about the opto-thermal (endo)vascular responses to selective photothermolysis, used as a default treatment modality for superficial vascular anomalies such as port wine stains, telangiectasias, and hemangiomas. In this preliminary study we present a novel microscopy technique for studying (endo)vascular laser-tissue interactions in vivo, in which conventional orthogonal polarized spectral (OPS) imaging is combined with darkfield (DF) illumination. DFOPS imaging of rat mesenteric vasculature irradiated at increasing powers revealed the following (tissular) responses: formation of translucent aggregates, retrograde flow, gradual and immediate hemostasis, reinstatement of flow, vessel disappearance, and perivascular collagen damage. DFOPS imaging therefore constitutes a useful tool for examining (endo)vascular events following selective photothermolysis.

OCIS codes: (170.0110) Imaging systems; (110.0180) Microscopy; (350.5340) Photothermal effects

References and links

1. D. W. Slaaf, G. J. Tangelder, R. S. Reneman, K. Jager, and A. Bollinger, "A versatile incident illuminator for intravital microscopy," Int. J. Microcirc. Clin. Exp. **6,** 391-397 (1987).
2. K. R. Mathura, G. J. Bouma, and C. Ince, "Abnormal microcirculation in brain tumours during surgery," Lancet **358,** 1698-1699 (2001).
3. F. A. Pennings, G. J. Bouma, and C. Ince, "Direct observation of the human cerebral microcirculation during aneurysm surgery reveals increased arteriolar contractility," Stroke **35,** 1284-1288 (2004).
4. P. E. Spronk, C. Ince, M. J. Gardien, K. R. Mathura, H. M. Oudemans-van Straaten, and D. F. Zandstra, "Nitroglycerin in septic shock after intravascular volume resuscitation," Lancet **360,** 1395-1396 (2002).
5. K. R. Mathura, K. C. Vollebregt, K. Boer, J. C. De Graaff, D. T. Ubbink, and C. Ince, "Comparison of OPS imaging and conventional capillary microscopy to study the human microcirculation," J. Appl. Physiol. **91,** 74-78 (2001).
6. W. Groner, J. W. Winkelman, A. G. Harris, C. Ince, G. J. Bouma, K. Messmer, and R. G. Nadeau, "Orthogonal polarization spectral imaging: a new method for study of the microcirculation," Nat. Med. **5,** 1209-1212 (1999).
7. S. Langer, P. Biberthaler, A. G. Harris, H. U. Steinau, and K. Messmer, "In vivo monitoring of microvessels in skin flaps: introduction of a novel technique," Microsurgery **21,** 317-324 (2001).

#5924 - $15.00 US Received 9 December 2004; revised 14 January 2005; accepted 19 January 2005

8. A. G. Harris, I. Sinitsina, and K. Messner, "Validation of OPS imaging for microvascular measurements during isovolumic hemodilution and low hematocrits," Am. J. Physiol. Heart Circ. Physiol. **282,** H1502-H1509 (2002).
9. S. Pahernik, A. G. Harris, M. Schmitt-Sody, S. Krasnici, A. E. Goetz, M. Dellian, and K. Messmer, "Orthogonal polarisation spectral imaging as a new tool for the assessment of antivascular tumour treatment in vivo: a validation study," Br. J. Cancer **86,** 1622-1627 (2002).
10. K. C. Vollebregt, K. Boer, K. R. Mathura, J. C. de Graaff, D. T. Ubbink, and C. Ince, "Impaired vascular function in women with pre-eclampsia observed with orthogonal polarisation spectral imaging," BJOG. **108,** 1148-1153 (2001).
11. H. Sherman, S. Klausner, and W. A. Cook, "Incident dark-field illumination: a new method for microcirculatory study," Angiology **22,** 295-303 (1971).
12. R. R. Anderson and J. A. Parrish, "Selective photothermolysis: precise microsurgery by selective absorption of pulsed radiation," Science **220,** 524-527 (1983).
13. M. M. Hamilton, "Laser treatment of pigmented and vascular lesions in the office," Facial Plast. Surg. **20,** 63-69 (2004).
14. S. Falati, P. Gross, G. Merrill-Skoloff, B. C. Furie, and B. Furie, "Real-time in vivo imaging of platelets, tissue factor and fibrin during arterial thrombus formation in the mouse," Nat. Med. **8,** 1175-1180 (2002).
15. E. D. Rosen, S. Raymond, A. Zollman, F. Noria, M. Sandoval-Cooper, A. Shulman, J. L. Merz, and F. J. Castellino, "Laser-induced noninvasive vascular injury models in mice generate platelet- and coagulation-dependent thrombi," Am. J. Pathol. **158,** 1613-1622 (2001).
16. W. I. Rosenblum, G. H. Nelson, B. Wormley, P. Werner, J. Wang, and C. C. Shih, "Role of platelet-endothelial cell adhesion molecule (PECAM) in platelet adhesion/aggregation over injured but not denuded endothelium in vivo and ex vivo," Stroke **27,** 709-711 (1996).
17. S. Mordon, S. Begu, B. Buys, C. Tourne-Peteilh, and J. M. Devoiselle, "Study of platelet behavior in vivo after endothelial stimulation with laser irradiation using fluorescence intravital videomicroscopy and PEGylated liposome staining," Microvasc. Res. **64,** 316-325 (2002).
18. W. Verkruysse, J. F. Beek, E. van Bavel, M. J. C. van Gemert, and J. Spaan, "Laser pulse impact on rat mesenteric blood vessels in relation to laser treatment of port wine stain," Lasers Surg. Med. **28,** 461-468 (2001).
19. O. T. Tan, D. Whitaker, J. M. Garden, and G. Murphy, "Pulsed dye laser (577 nm) treatment of portwine stains: ultrastructural evidence of neovascularization and mast cell degranulation in healed lesions," J. Invest. Dermatol. **90,** 395-398 (1988).
20. O. T. Tan, J. G. Morelli, D. Whitaker, J. Boll, and G. Murphy, "Ultrastructural changes in red blood cells following pulsed irradiation in vitro," J. Invest. Dermatol. **92,** 100-104 (1989).
21. J. F. Black and J. K. Barton, "Chemical and structural changes in blood undergoing laser photocoagulation," Photochem. Photobiol. **80,** 89-97 (2004).
22. K. Suthamjariya, W. A. Farinelli, W. Koh, and R. R. Anderson, "Mechanisms of microvascular response to laser pulses," J. Invest. Dermatol. **122,** 518-525 (2004).
23. J. Lindert, J. Werner, M. Redlin, H. Kuppe, H. Habazettl, and A. R. Pries, "OPS imaging of human microcirculation: a short technical report," J. Vasc. Res. **39,** 368-372 (2002).
24. J. K. Barton, D. Popok, and J. F. Black, "Thermal analysis of blood undergoing laser photocoagulation," IEEE J. Sel. Topics Quant. Electron. **7,** 936-943 (2001).
25. J. K. Barton, G. Frangineas, H. Pummer, and J. F. Black, "Cooperative phenomena in two-pulse, two-color laser photocoagulation of cutaneous blood vessels," Photochem. Photobiol. **73,** 642-650 (2001).
26. K. Takeda, A. Wada, K. Yamamoto, Y. Moriyama, and K. Aoki, "Conformational change of bovine serum albumin by heat treatment," J. Protein Chem. **8,** 653-659 (1989).
27. A. R. Tall, D. M. Small, G. Shipley, and R. S. Lees, "Apoprotein stability and lipid-lipid protein interactions in human plasma high density lipoproteins," Proc. Nat. Acad. Sci. **72,** 4940-4942 (1975).
28. M. Heger, J. F. Beek, N. I. Moldovan, C. M. A. M. van der Horst, and M. J. C. van Gemert, "Towards optimization of selective photothermolysis: prothrombotic pharmaceutical agents as potential adjuvants in laser treatment of port wine stains. A theoretical study," Thromb. Haemost. **92,** 242-257 (2005).
29. S. P. Jackson, W. S. Nesbitt, and S. Kulkarni, "Signaling events underlying thrombus formation," J. Thromb. Haemost. **1,** 1602-1612 (2003).
30. O. Genevois, M. Paques, M. Simonutti, R. Sercombe, J. Seylaz, A. Gaudric, J. P. Brouland, J. Sahel, and E. Vicaut, "Microvascular remodeling after occlusion-recanalization of a branch retinal vein in rats," Invest. Ophthalmol. Vis. Sci. **45,** 594-600 (2004).
31. S. Thomsen, "Pathological analysis of photothermal and photomechanical effects of laser-tissue interactions," Photochem. Photobiol. **53,** 825-835 (2001).
32. R. Dong, X. Yan, X. Pang, and S. Liu, "Temperature-dependent Raman spectra of collagen and DNA," Spectrochim. Acta A **60,** 557-561 (2004).
33. T. V. Belopolskaya, G. I. Tsereteli, N. A. Grunina, and O. L. Vaveliouk, "DSC study of the postdenatured structures in biopolymer-water systems," J. Therm. Anal. Calorim. **62,** 75-88 (2000).
34. S. S. Chen, N. T. Wright, and J. D. Humphrey, "Heat-induced changes in the mechanics of a collagenous tissue: isothermal free shrinkage," J. Biomech. Eng. **119,** 372-378 (1997).

#5924 - $15.00 US Received 9 December 2004; revised 14 January 2005; accepted 19 January 2005

1. Introduction

Orthogonal polarized spectral (OPS) imaging is a polarized light-based microscopic technique for intravital, non-invasive visualization of superficially located microcirculation [1]. OPS has recently been introduced in the clinical setting to image distinctive microvascular and hematological pathologies associated with different disease states, including (cardio)vascular diseases, cancer, and sepsis [2-4]. The imaging technique allows the observation of vascular structures and endovascular constituents (red blood cells and leukocytes) at high contrast [5], and facilitates quantitative measurements of physiological parameters (red blood cell velocity, vasomotion) as well as pathophysiological conditions (ischemia/reperfusion, hemorrhage, tumor angiogenesis) without requiring contrast enhancers or fluorescent dyes [3,6-10]. In OPS imaging, vascularized tissue is illuminated with linearly polarized light, while the remitted light is imaged through an analyzer (second polarizer) oriented orthogonally to the polarizer. The polarized source light is passed through a green spectral filter (548 nm) to ensure significant absorption by hemoglobin (Hb) and oxy-hemoglobin (HbO_2). In non-absorbing tissue, such as perivascular tissue, the light undergoes multiple scattering events that randomize the plane of polarization. The depolarized scattered light back-illuminates the chromophore-containing red blood cells in the foreground, providing negative contrast with respect to vascular structures, i.e. the imaged vessels appear black against a light background. The remitted light is subsequently collected by the same objective lens and guided through the analyzer onto a CCD camera to comprise the image [1]. As opposed to a shared optical path for the source light and remitted light in the conventional OPS systems, darkfield (DF) OPS systems project the illumination concentrically on the tissue outside the field of view of the image capturing device [11] by means of an opening in the middle of the beam splitter, and collect the remitted light through the central pathway (see Fig. 1). As a result, the DF means of illumination significantly enhances contrast and improves the quality of the OPS images.

Here we report on the utility of DFOPS in studying endovascular laser-tissue interactions as they relate to selective photothermolysis, a process that relies on the conversion of radiant energy to heat by $Hb(O_2)$, and the ensuing thermal necrosis of blood and vascular tissue resulting from heat diffusion [12]. By employing a wavelength substantially absorbed by $Hb(O_2)$ at a pulse duration that matches the thermal relaxation time of the target vasculature, i.e. the time required for a heated vessel to lose 50% of its thermal energy, vessels can be selectively damaged without affecting perivascular tissue. Selective photothermolysis constitutes the default treatment modality in the non-invasive removal of a broad array of superficial vascular anomalies, including port wine stains, hemangiomas, and telangiectasias [13]. The acute and chronic inflammatory responses triggered by laser-induced endovascular damage lead to vascular remodeling processes that result in lesional clearance. The exact mechanisms underlying the (endo)vascular responses to laser irradiation have not been extensively elucidated, primarily due to the fact that only few in vivo techniques have been developed to categorically examine these phenomena [14-18]. Moreover, most of these laser-induced vessel wall injury models [14-16] focus the laser beam directly on the endothelial layer, creating a damage profile that differs from selective photothermolysis in that the chromophore-containing red blood cells are circumvented as thermal catalysts and heat diffusion is an irrelevant factor. As a result, the formation of coagula consisting of thermally denatured circulatory cells and plasma proteins [19-21] is excluded from the damage profile in these models. In a recent intravital study on hamsters, Suthamjariya and associates [22] showed that during the laser pulse, (endo)vascular events occur in the following order with increasing intraluminal fluences (J/cm^2): 1) thermal coagulation of blood; 2) vasoconstriction; 3) thread-like appearance of the irradiated vessel segment; 4) vessel disappearance; 5) intravascular cavitation expanding along vessel lumen; 6) violent, bubble-like cavitation; 7) vessel wall rupture and hemorrhage; and 8) denaturation and shrinkage of perivascular collagen. However, their setup did not permit the visualization of specific laser-induced

#5924 - $15.00 US Received 9 December 2004; revised 14 January 2005; accepted 19 January 2005

effects on local hemodynamics, i.e. changes in direction and velocity of flow. Moreover, the protocol focused on the phenomena occurring during selective photothermolysis, and did not incorporate post-irradiation events such as reinstatement of flow and latent hemostasis. This preliminary study aims to elucidate the (endo)vascular events following laser irradiation and serves as a proof-of-principle for the utility of DFOPS in researching laser-tissue interactions in vivo.

2. Materials and methods

2.1 Preparation of animals

The protocol was approved by the Animal Ethics Committee of the Academic Medical Center. Five male Wistar rats (Charles River Laboratories, Maastricht, The Netherlands), weighing 250-300 g, were deprived of food for 24 hours before the operation to reduce intestinal peristalsis. Rats were anesthetized by intraperitoneal injection of Ketamine (90 mg/kg), Medetomedine (0.5 mg/kg), and Atropine (0.05 mg/kg). Each animal was mechanically ventilated and placed on a heated stage to maintain body temperature. Vital signs were continually monitored. A medial laparotomy was performed to exteriorize an intestinal loop, which was secured on an elevated platform positioned adjacently to the incision site so as to enable optimal placement of the intestine and the DFOPS probe. Excessive desiccation of internal and exposed organs was alleviated by applying Ringer's solution preheated to 37˚C. During surgery and DFOPS imaging anesthesia was continuously maintained by intravenous injection of Ketamine (50 mg/kg/hr) with an infusion pump. At the end of the experiments the rats were sacrificed by intravenous administration of high doses KCl.

2.2 DFOPS imaging and video editing

A Cytoscan E-II Backfocus type device (Cytometrics, Philadelphia, PA) was used for DFOPS imaging. The module emits light at a wavelength of 548 nm at tunable intensities. The DFOPS probe was secured in a vertically adjustable holder to ensure steadfast imposition of the sterile plastic cap surrounding the tip of the light guide on the tissue with minimal impediment of blood flow. Suitable microvascular networks in the mesenteric sheath enveloping the large intestine were identified by gently moving the Cytoscan probe over the tissue. A 10x objective was used for image capture. In vivo, the typical depth of focus is approximately 200 μm at a resolution of 1 μm^2 per CCD pixel, allowing visualization of individual red blood cells and leukocytes at flow velocities below 1 $mm \cdot s^{-1}$ [23]. The built-in CCD chip has a data acquisition rate of 25 frames per second. All data were recorded on a Sony DSR-20P digital video recorder and visualized on a Sony PVM 97 monitor. For optimal visualization of laser-induced effects, the contrast of the videos in Figs. 3 and 6 was also inverted using Adobe Premiere Pro 1.5 software. The actual (unedited) videos in DV.avi format have been posted on our OPS imaging website, http://www.opsimaging.net.

2.3 Laser irradiation

A frequency-doubled Nd:YAG laser (Alcon Laboratories, model Ophthalas 532 EyeLite, Forth Worth, TX) was employed to induce (endo)vascular damage in selected microvascular networks. The laser emits a wavelength of 532 nm, corresponding to a significant absorption coefficient of $Hb(O_2)$ for selective photothermolysis. An engineered opening in the side of the bottom part of the protective plastic cap allowed insertion and positioning of the laser probe without interfering with the visual field of DFOPS. Proper targeting was achieved by manually guiding the aiming beam of the laser to the region of interest, as confirmed by the highly reflective spot on the video image (see movies Figs. 4 and 6). It should be noted that in the actual experiments, the laser probe had to be inserted at variable angles, causing the spot to become elliptical rather than circular and the irradiances to vary across the beam diameter.

#5924 - $15.00 US Received 9 December 2004; revised 14 January 2005; accepted 19 January 2005

The measured spot sizes ranged from 0.3 mm^2 to 0.4 mm^2. The minimum laser power required for visible (endo)vascular effects was initially empirically determined by increasing power by 100 mW increments while keeping pulse duration constant at 500 ms. DFOPS imaging of laser-irradiated vasculature was only performed above the established threshold power settings. The imaged vascular region was irradiated once unless otherwise noted in the text.

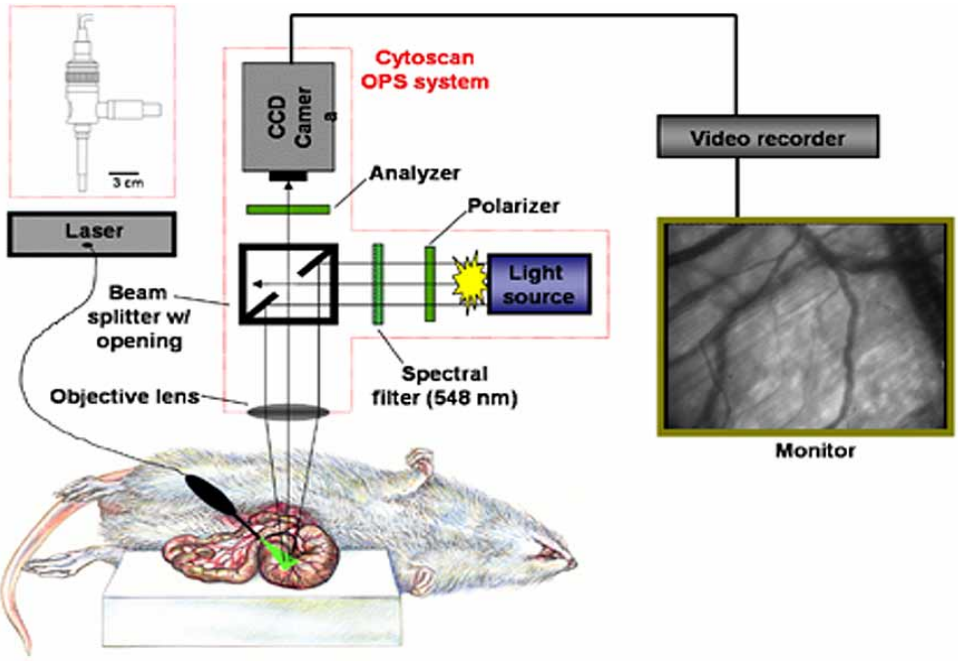

Fig. 1. Diagram of the experimental setup. The Cytoscan probe (insert top left) is positioned onto an exteriorized rat large intestine. Source light incident on tissue is passed through a polarizer and a green spectral filter (548 nm). Remitted light is guided through an orthogonally oriented polarizer (analyzer) to a CCD camera by a beam splitter, and the images are video-recorded. A frequency-doubled Nd:YAG laser (532 nm) is used to inflict photothermal damage during DFOPS imaging.

2.4 DFOPS imaging and light microscopy of laser-induced thermal coagula in vitro

To ascertain whether the laser-induced, blood-borne translucent material (that was ubiquitously present in all irradiated vasculature imaged with DFOPS) was composed of coagulated red blood cells, we performed DFOPS analysis on irradiated porcine whole blood in vitro. The blood was collected into plastic tubes containing an anticoagulant mixture of citrate, phosphate, and dextrose. Small cuvettes (average length 1.18 mm, width 0.40 mm, depth 20.8 mm) were constructed by gluing glass cover slips surface to surface onto a microscope slide using UV glue. The blood was deposited at the superior opening of the cuvette and allowed to move into the cuvette by capillary action. The cuvettes were irradiated with the previously employed frequency doubled Nd:YAG laser at a constant pulse duration (500 ms) and increasing power: 1000 mW (4 cuvettes); 1500 mW (4 cuvettes); and 2000 mW (4 cuvettes). The laser probe was firmly secured in a specially designed holder to ensure an invariable distance between the probe tip and the sample, producing a spot size of 2.7 mm^2. The radiant exposures for each laser setting were measured using a power meter with a thermal surface absorber (Ophir Optronics, Jerusalem, Israel). Ten measurements were made for each laser setting and the values were averaged. The maximum and minimum values were excluded from the radiant exposure calculations. Immediately after irradiation, the cuvettes

#5924 - $15.00 US Received 9 December 2004; revised 14 January 2005; accepted 19 January 2005

were examined by DFOPS imaging and light microscopy (Nikon, model Eclipse E600, Bunnik, The Netherlands). For DFOPS imaging, the cuvettes were placed on thick white paper to ensure maximum reflection of light and illumination of the coagulum.

3. Results

Screening of vascular networks occurred by laterally moving the OPS probe over the tissue. Only those regions in which the vasculature was of relatively small diameter (up to 50 μm) and superficially located were selected for OPS imaging and laser irradiation. Densely vascularized and optically shielded regions (by vessel superimposition) were avoided to ensure maximum remission of scattered light.

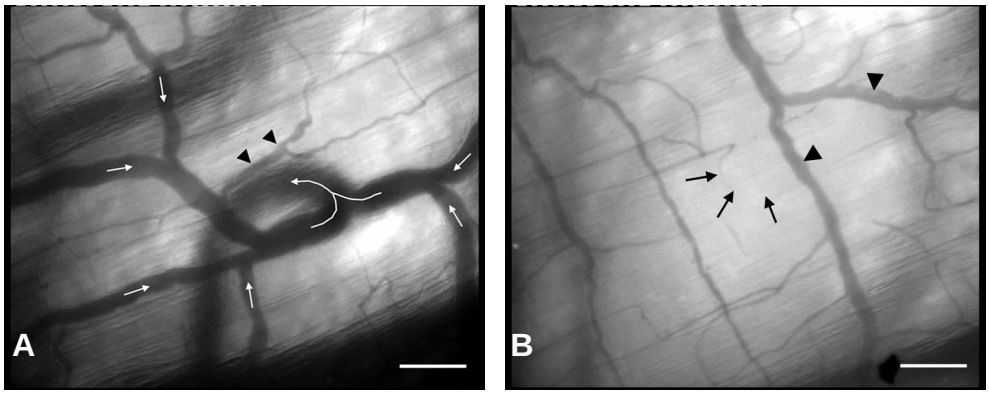

Fig. 2. OPS imaging of superficially located microcirculation in the large intestine of a rat. (a) (2.2 MB) Movie: Hierarchical organization of mesenteric vasculature (14.6 MB version). Arrows indicate direction of flow, arrowheads indicate vessel segment with clearly visible leukocyte rolling. (b) (1.4 MB) Movie: Leukocyte rolling and red blood cell-devoid strips of plasma (14.5 MB version). Arrows indicate translucent strips of plasma, arrowheads point to sites of clearly visible leukocyte rolling. Scale bar = 100 μm. The original movies in DV.avi format can be downloaded from http://www.opsimaging.net.

Based on the imaged vessel dimensions, direction of flow (arrows), and anastomotic patterns in Fig. 2(a), it is evident that the superficial vascular architecture in the transparent mesenteric sheath is primarily composed of capillaries and collecting venules and veins. The latter connect to the deeper vascular plexus through an intermediary descending vessel. In some of the smaller venules and capillaries, flowing red blood cells can be identified, whereas the flow velocity and optical density of the chromophores in the larger vessels are too high for visualization of individual cells. Occasionally, the red blood cells passing through capillaries are separated by long strips of pellucid plasma (Fig. 2(b), arrows). Leukocyte rolling, a process in which leukocytes transiently tether to the intimal layer during flow, can be observed in the vasculature as white (translucent) cells moving along the vessel-tissue interface (Figs. 2(a) and 2(b), arrowheads). Finally, rhythmic pulsation is seen in the intermediary vessel and vasculature of the deeper plexus (Fig. 2(a), movie).

To examine the photothermal responses in vessels, the imaged tissue was irradiated with a frequency-doubled Nd:YAG laser at powers above the threshold for visible damage (~ 800 mW). Laser power was incrementally amplified to induce different damage profiles associated with rising volumetric heat production.

#5924 - $15.00 US Received 9 December 2004; revised 14 January 2005; accepted 19 January 2005

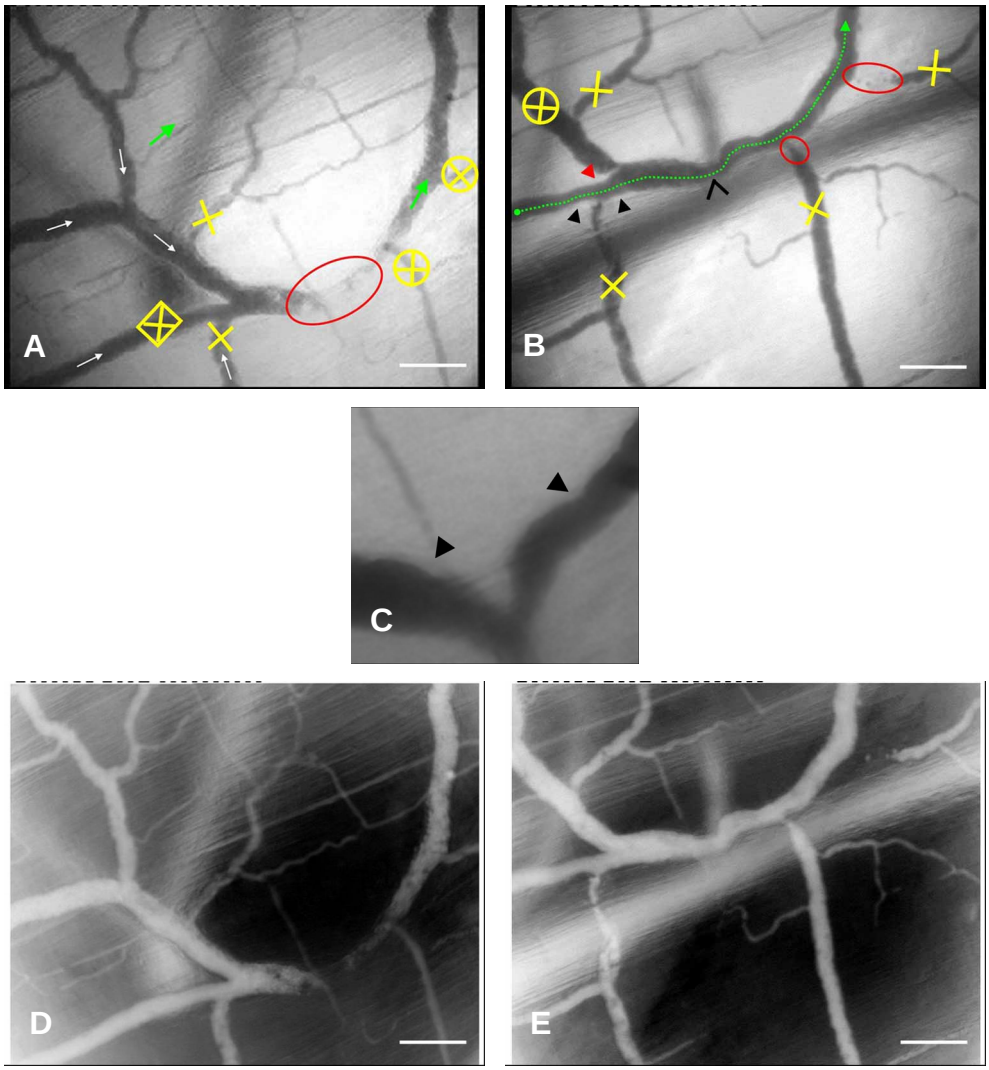

Fig. 3. (a) (1.5 MB) Movie: Formation of translucent matter in laser-irradiated microcirculation (14.0 MB version). The laser was set to a power of 1000 mW, 500 ms pulse duration, and a spot size of 0.35±0.05 mm^2. Laser irradiation (white screen in movie) induced the formation of translucent matter (encircled) in the vasculature imaged in Fig 2(a). All yellow crosses designate hemostatic vessels after lasing, white arrows indicate direction of flow before irradiation, and green arrows signify retrograde flow after irradiation. (b) (2.5 MB) Movie: Vasculature in (a), two minutes after laser irradiation (9.3 MB version). The open arrowhead marks the encircled area in (a), the green arrow indicates main flow path of blood, all yellow crosses signify hemostatic vessels, black arrowheads designate translucent, endoluminal obstructions, red arrowhead designates detaching translucent matter, and the red circles demarcate translucent vessel segments. (c) Encircled area in (a) enlarged. Arrowheads point to translucent material attached to the vessel wall. (d) (2.4 MB) Movie: Fig. 3(a), inverted contrast (14.4 MB version). (e) (2.3 MB) Movie: Fig. 3(b), inverted contrast (14.6 MB version). Scale bar = 100 µm. The original movies in DV.avi format can be downloaded from http://www.opsimaging.net.

The movie in Fig. 3(a) shows that translucent matter is formed immediately after the 1000 mW, 500 ms laser pulse. The translucent matter is predominantly concentrated in the section where the two main venules connect to the descending, intermediary vessel (Fig. 3(a), encircled). This point of confluence (Fig. 3(a), encircled) appears constricted after the pulse,

#5924 - $15.00 US Received 9 December 2004; revised 14 January 2005; accepted 19 January 2005

and the descending vessel is no longer in the field of view, although several seconds later it partially reappears. The vast majority of the translucent material is hemodynamically removed in retrograde direction through the right main venule and its two branching vessels (Fig. 3(a), encircled crosses), although circulation in the latter and other vessels (Fig. 3(a), all crosses) eventually ceases. A smaller portion of the material is initially propelled in the opposite direction into the left main venule and its superior branching vessel, but ultimately most of the translucent material is removed via the junction (Fig. 3(a), encircled) and the right main venule. During this process, the larger translucent bodies occasionally fragment and separate. In addition to the right main venule, the direction of flow has reversed in a feeding venule that anastomoses to a branching vessel of the left main venule (Fig. 3(a), green arrows). Furthermore, translucent matter has attached to the vessel wall immediately after the pulse in the vessel segments adjacent to the junction (Fig. 3(c), arrowheads). Laser irradiation also induced a substantial reduction in flow velocity in the imaged vasculature.

Two minutes after irradiation (Fig. 3(b)), flow is fully reinstated through one of the vessels that had become hemostatic immediately after lasing (Fig. 3(a), boxed cross), while flow in the larger branch of the left main vessel (Fig. 3(b), encircled cross) has virtually been reduced to null. The smaller branch of the left main vessel (Fig. 3(a), boxed cross) and the right main vessel seem to comprise the main circulatory pathway in the photothermally affected tissue (Fig. 3(b), green dotted line). All the other vessels have undergone complete hemostasis (Fig. 3(b), all crosses). At the connecting ends of the two upstream branching venules (Fig. 3(a), encircled crosses), translucent material has gradually accumulated and occupies a relatively large portion of the lumen (Fig. 3(b)), red circles). Translucent material has also formed stable adhesion points on the inner vessel wall, causing mild venular stenosis (Fig. 3(b), arrowheads). These obstructions were not present immediately (Fig. 3(a), movie) or 50 seconds after the laser pulse (movie, http://www.opsimaging.net). Moreover, at the intersection where the two venules conjoin to comprise the left main venule (Fig. 3(b), red arrowhead), translucent material transiently conglomerates, detaches from the ridge, and is subsequently removed by the circulation.

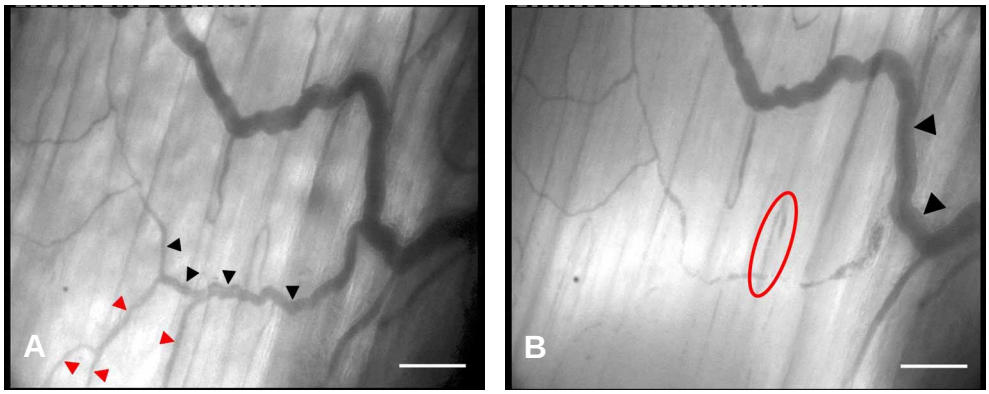

Fig. 4. (1.3 MB) Movie: Vessel disappearance following laser irradiation (14.2 MB version). The laser was set to a power of 1500 mW and 500 ms pulse duration with a spot size of 0.35±0.05 mm^2. (a) shows a video frame right before laser irradiation (white screen in movie), and (b) displays a video frame immediately after the laser pulse. Small arrowheads in (a) indicate affected vessels in (b), large arrowheads in (b) designate unaffected vessel, and circle marks intact loop vessel. Scale bar = 100 µm. The original movie in DV.avi format can be downloaded from http://www.opsimaging.net.

Laser irradiation at 1500 mW, 500 ms, and a spot size of 0.35±0.05 mm^2 inflicted a differential response in the vasculature situated within the irradiated zone (Fig. 4(a), arrowheads). A pre-irradiation video frame (A) is juxtaposed to a post-irradiation video frame

#5924 - $15.00 US Received 9 December 2004; revised 14 January 2005; accepted 19 January 2005

(B) in Fig. 4. The pulse induced vessel disappearance in the smaller diameter vessels (Fig. 4(a), red arrowheads), whereas the larger diameter vessel (Fig. 4(a), black arrowheads) primarily underwent vasoconstriction. Translucent material is present in the larger diameter vessel (Fig. 4(a), black arrowheads) immediately after the laser pulse. Flow persisted in the right half of this vessel due to the intact state of the loop structure (Fig. 4(b), encircled) and the large venule (Fig. 4(b), arrowheads), albeit at impaired levels. Influx of additional translucent material into the larger diameter vessel in the irradiated zone (Fig. 4(a), black arrowheads) occurred via the loop structure, whereas the large venule (Fig. 4(b), arrowheads) facilitated the drainage of the translucent matter.

Two and a half minutes after irradiation (Fig. 5, movie), the flow velocity is significantly reduced in the large venule that initially remained unaffected by the laser pulse (Fig. 4(b), arrowheads), although we cannot rule out that this may have been due to laser irradiation of other, nearby vascular structures (data not shown). At three seconds into the movie (Fig. 5, movie), the vein spontaneously ruptures without any exogenous stimuli, and red blood cells gradually extravasate into the perivascular space. After extravasation the vessel wall can be visualized as the pellucid interface between the small hematoma and the blood-filled column.

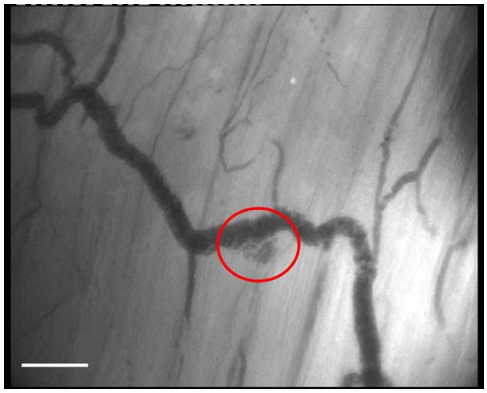

Fig. 5. (1.5 MB) Movie: Acute hemorrhage in partially affected vessel 2.5 minutes after laser irradiation at 1500 mW, 500 ms pulse duration, and a 0.35±0.05 mm^2 spot size (10.0 MB version). Hemorrhage (encircled) occurs from the large vessel depicted in Fig. 4 without exogenous stimuli. Scale bar = 100 µm. The original movie in DV.avi format can be downloaded from http://www.opsimaging.net.

The vasculature imaged in Figs. 4 and 5 was irradiated a second time at 2000 mW, 500 ms, and a 0.35±0.05 mm^2 spot size, 3:45 minutes after the first laser pulse. Figs. 6(a) and 6(c) show the pre- and post-irradiation video frames, respectively. Interestingly, the vessel that had constricted after the first laser pulse (Fig. 4(a), black arrowheads) had reverted to its original diameter before the second laser pulse (Fig. 6(a), arrowheads). As in previous images, laser irradiation induced differential responses in the targeted vasculature, ranging from the formation of translucent material (Fig. 6(b), red arrowhead) and retrograde flow (Fig. 6(b), arrow) at the periphery of the laser beam to hemostasis, vasoconstriction, and vessel disappearance (Fig. 6(b), inside the dotted line) in the center of the laser beam. The pulse also markedly decreased the reflectivity of the mesenteric sheath in the irradiated region, which coincides with the region illuminated by the aiming beam. We purposefully retained the aiming beam on the irradiated site for one second after the laser pulse so as to demonstrate the overlap (see movie). A large part of the hemorrhaged vascular segment (Fig. 5, encircled) has disappeared, whereas the hemostatic vessel (Fig. 6(a), arrowheads), which is also located in the central region of the beam, has vasoconstricted. The distance between these vessels markedly decreased following irradiation. The pulse did not impinge on the extravasated red blood cells (Fig. 6(b), black arrowhead). Furthermore, the translucent section of the vertically

#5924 - $15.00 US Received 9 December 2004; revised 14 January 2005; accepted 19 January 2005

oriented vessel segment in Fig. 6(a) has been filled by chromophore-containing red blood cells instantaneously after laser irradiation (Fig. 6(b), encircled). At the periphery of the irradiated region, a large body (~ 120 μm) of translucent material has formed (Fig. 6(b), red arrowhead). This material does not adhere to the vessel wall as it moves through the column with the (residual) blood flow. With time it is forced apart by the influx of blood via the two small capillaries that connect superiorly to the vessel segment (movie, http://www.opsimaging.net). Fourteen seconds after the laser pulse (Fig. 6(a), movie) the translucent material fragments and the smaller top portion is removed by the vessel with the reversed flow direction (Fig. 6(b), arrows). Interestingly, the vessel segment tapers as it intersects with the region of collagen damage, marking the boundary of the disappeared vessel, but distends when blood is gradually infused (movie).

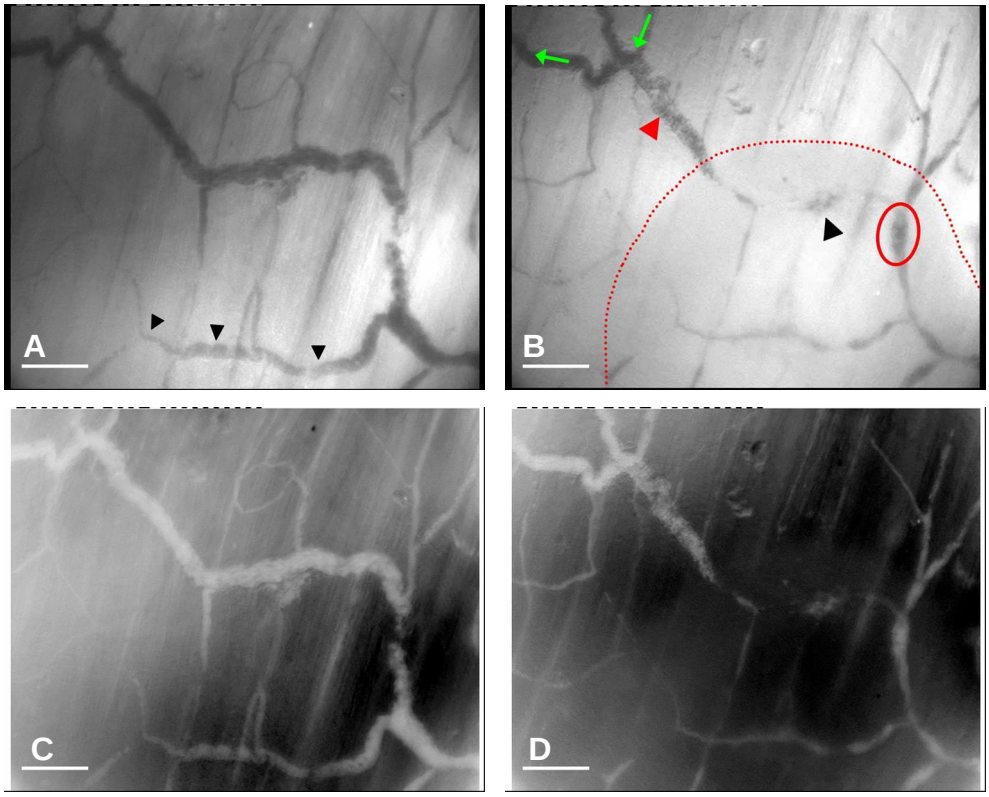

Fig. 6. (a) (1.3 MB) Movie: Disappearance of partially affected vessels following a second laser pulse (9.7 MB version). Vessels from Figs. 4 and 5 were irradiated again 3:45 minutes after the first laser pulse. The laser was set to maximum power (2000 mW) at 500 ms pulse duration and a spot size of 0.35±0.05 mm^2. (a) shows a video frame right before laser irradiation (white screen in movie), and (b) displays a video frame immediately after the laser pulse. The demarcated higher order damage region (Fig. 6(b), dotted line) corresponds to the center of the beam profile. Vessel marked by small arrowheads in (a) represents the similarly marked vessel in Fig. 4(a). In (b), black arrowhead indicates hemorrhage, red arrowhead designates translucent material, and green arrows signify retrograde flow. (c) (2.4 MB) Movie: Fig. 6(a), inverted contrast (14.6 MB version). (c) shows an inverted contrast video frame right before laser irradiation (black screen in movie), and (d) displays an inverted contrast video frame immediately after the laser pulse. Scale bar = 100 μm. The original movies in DV.avi format can be downloaded from http://www.opsimaging.net.

Several studies have shown that thermal coagula form during selective photothermolysis [19,21,22,24]. These coagula, consisting of agglutinated thermolysed red blood cells [19,21],

#5924 - $15.00 US Received 9 December 2004; revised 14 January 2005; accepted 19 January 2005

either adhere to the vessel wall or embolize following a laser pulse [19,22]. The optical properties of thermal coagula have been spectroscopically determined in vitro [25]. At 550 nm wavelength (approximately equivalent to the wavelength of the DFOPS light source), blood coagula elicit a reduced transmission, increased absorption and scattering coefficients, but no changes in reflectance [25] in comparison to uncoagulated whole blood. Based on the optical characteristics of thermal coagula, the translucent nature of the material observed in the laser-irradiated vasculature suggests that the material imaged with DFOPS is not composed of photocoagulated red blood cells. To demonstrate this experimentally, thermal coagula were induced in glass cuvettes at the laser parameters used in the in vivo experiments and subsequently imaged with DFOPS and light microscopy. Figures 7(a) and 7(b) show thermal coagula induced at 500 ms pulse duration and a power of 1000 mW, imaged with light microscopy (magnification 4x) and DFOPS (magnification 10x), respectively. Similarly, Figs. 7(c) and 7(d) show coagula created at 500 ms pulse duration and power of 1500 mW. No coagula were created at maximum power settings (500 ms, 2000 mW) because the laser pulse consistently triggered explosive expulsion of blood from the cuvette. Laser powers of 1000, 1500, and 2000 mW at 500 ms pulse duration correspond to average irradiances (±SD) of 58 (±3), 86 (±6), and 114 (±2) $W \cdot cm^{-2}$. The in vitro generated thermal coagula appear black (negative contrast) in the DFOPS images, meaning that the source light at 548 nm wavelength is absorbed. These findings are in agreement with the spectroscopic data published by Barton *et al.* [25].

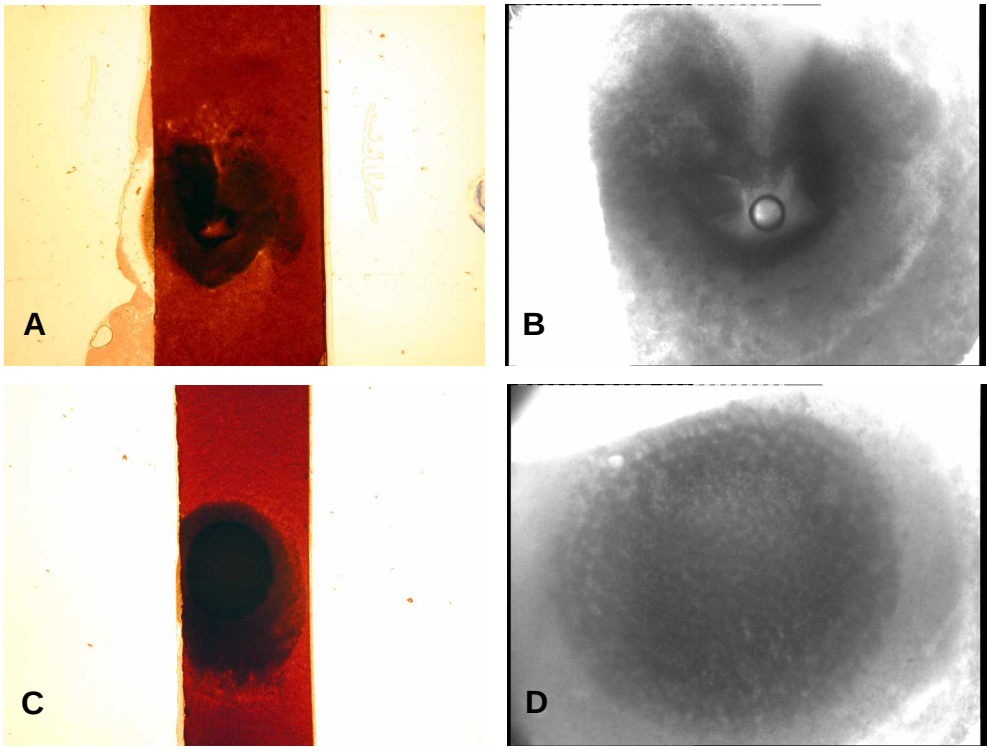

Fig. 7. (a) Light microscopic image of a laser-induced coagulum in vitro (532 nm, 500 ms, 1000 mW). The red column represents the blood-filled cuvette, the coagulum appears black. Original magnification x4. (b) Coagulum in (a) imaged with DFOPS. Original magnification x10. (c) Light microscopic image of a laser-induced coagulum in vitro (532 nm, 500 ms, 1500 mW). The red column represents the blood-filled cuvette, the coagulum appears black. Original magnification x4. (d) Coagulum in (c) imaged with DFOPS. Original magnification x10.

#5924 - $15.00 US Received 9 December 2004; revised 14 January 2005; accepted 19 January 2005

4. Discussion

In this preliminary study we have demonstrated, for the first time, that DFOPS imaging constitutes a useful tool for studying (endo)vascular laser-tissue interactions by selective photothermolysis in vivo. By using linearly polarized light at a wavelength that is well absorbed by $Hb(O_2)$ in a darkfield configuration, the vascular architecture, flow distribution, and cellular constituents can be imaged at high contrast while specular reflection is eliminated by the orthogonally oriented analyzer. Since the technique is based on spectral imaging at an absorption peak of Hb, any laser-induced shifts in the spatial distribution of the chromophore-containing red blood cells or aggregation/precipitation of translucent intraluminal material are immediately registered. A recent study by Suthamjariya *et al*. [22] evinced the events that occur during the laser pulse as a function of fluence rates (or volumetric heat production) using light microscopy. Our DFOPS imaging study, although preliminary, complements Suthamjariya *et al.'s* research by focusing on the (endo)vascular events following laser irradiation of rat mesenteric vessels.

The most striking event that occurred at all laser powers was the formation of translucent aggregates immediately after laser irradiation. At higher laser powers (1500 and 2000 mW), the translucent aggregates formed predominantly at the periphery of the irradiated region. This lower order damage effect at the periphery of the irradiated zone (Fig. 6(b)) may be ascribed to the Gaussian power distribution of the laser beam. Most of the translucent aggregates were blood-borne (Figs. 3, 4, and 6), but occasionally the translucent material attached to the vessel wall either immediately after the pulse (Fig. 3(c), arrowheads) or during later stages (Fig. 3(b), black and red arrowheads). In vitro DFOPS imaging of laser-induced coagula ruled out that the translucent material is composed of chromophore-containing thermolysed cells, which is corroborated by the spectroscopic analysis performed by Barton *et al*. [25]. Unfortunately, DFOPS imaging at this magnification is limited insofar as the translucent material cannot be conclusively characterized and no irrefutable distinction can be made between the various translucent constituents. Despite these limitations, it is arguable that the blood-borne translucent bodies are comprised of thermally denatured and precipitated plasma proteins, which have a lower irreversible denaturation threshold than lipoproteins or cell membranes [20,26] due to the lack of thermodynamically stabilizing phospholipids [27]. Generated intraluminal isotherms may therefore be subcritical for thermolysis and agglutination (>80˚C) [24] of red blood cells, yet exceed the threshold values for irreversible plasma protein denaturation (i.e., >45˚C for serum albumin) [26]. This would explain why these aggregates can form without coagulum-induced emphraxis of the vessel lumen (Fig. 3(a)). The translucent matter that was attached to the vessel wall immediately after the laser pulse (Fig. 3(c)) may also consist of denatured plasma proteins or non-chromophore-containing plasma cells chemically affixed to the endothelial monolayer (see theoretical study by Heger *et al*. [28]), whereas the translucent adherent material that developed several minutes after the laser pulse (Fig. 3(b), black and red arrows) may represent sites of platelet aggregation. These postulations are justified by the fact that the development of a nidus (biochemical response) takes several seconds to complete [29], whereas creation of non-embolizing (sub)occlusive thermal coagula (photothermal response) occurs during and immediately after the laser pulse [21,22,24].

Laser irradiation of the intestinal vasculature also triggered hemodynamic changes that were not necessarily confined to the irradiated zone. Irradiation at 500 ms and 1000 mW induced an instantaneous reduction in blood flow velocity, gradual hemostasis, and retrograde flow in directly and indirectly affected vasculature. The observed retrograde flow (Figs. 3(a) and (b) green arrows) has also been reported by Genevois and colleagues [30] during laser-induced branch retinal vein occlusion. We propose that this may be a result of circulatory obstructions in the laser-irradiated vessel segment(s), whereby blood flow in the intact vasculature that is connected to the obstructed draining vessel is redirected into the vessel

#5924 - $15.00 US Received 9 December 2004; revised 14 January 2005; accepted 19 January 2005

with the least pressure resistance. In Fig. 3(a), for instance, obstruction of the (disappeared) intermediary descending vessel segment may have caused an acute collision of the two opposing bloodstreams at the anastomotic junction, forcing the blood to flow against the lowest pressure gradient, i.e. up the right main venule (Fig. 3(a), green arrow). Similarly, vessel disappearance in Fig. 6 completely abrogated fluency in the vessel segment containing the translucent aggregates (Fig. 6(b), red arrow). This in turn may have lead to a reorganization of flow directionality in the merging vessels pictured in the top left quadrant of Fig. 6(b) (green arrows). An interesting development associated with hemostasis was the accumulation of translucent material at the branching junctions of the hemostatic vessels that anastomosed to patent vasculature (Fig. 3(b), encircled). The translucent vessel segment in Fig. 6(a) (encircled in Fig. 6(b)) gradually developed by the same dynamics (movie, http://www.opsimaging.net). Albeit the composition of the translucent material is unknown, we speculate that hemostatic vascular segments connected to non-obstructed vessels accumulate plasma and chromophore-lacking cells such as platelets and leukocytes. Rheologically, platelets and leukocytes are primarily found near the blood-endothelium interface, whereas the red blood cells predominantly occupy the center of the bloodstream. The position of these cells, perhaps in coaction with increased blood pressure in the patent vessel resultant from the obstruction of draining sites, makes it likely that these cells and plasma are impelled into the hemostatic branching vessels. Furthermore, a vessel in which circulation ceased after the laser pulse regained flow two minutes after irradiation (Fig. 3(b), boxed cross), showing the potential of vessels to become patent within minutes after laser-induced hemostasis. Unfortunately, it is difficult to account for most of these (photothermally-modulated) hemodynamic effects because the events that take place in the vasculature outside the field of view cannot be considered.

The higher order fluence-dependent damage profiles observed during DFOPS imaging included vessel disappearance [22] and alterations in the reflectivity of the irradiated mesenteric sheath. According to Suthamjariya [22], vessel disappearance results either from midpoint separation and subsequent retraction of a formed coagulum or intravascular cavitation expanding along the vessel lumen. Both events occur during the laser pulse, hence the underlying mechanisms responsible for the vessel disappearance in Figs. 4 and 6 cannot be established by DFOPS imaging. Inasmuch as the vessel wall is devoid of chromophores, it is also difficult to ascertain whether the disappeared vessel segments contain pellucid material, or whether the vessel wall has collapsed due to the pressure gradient created by a retracting coagulum or expanding bubble. It is arguable that the vessel wall in Fig. 6 collapsed during the laser pulse, given that the disappeared vessel segment is gradually filled with blood at its left extremity (Fig. 6(b), between the red and black arrowhead at the height of the dotted line), causing the diameter of the column to widen and its morphology to become outlined. This is further reinforced by the possibility that red blood cells were forced into the pellucid section (Fig. 6(b), encircled) upon vascular collapse during the laser pulse, replacing the initial translucent material. The absence of thermal mass (red blood cells) in this translucent segment likely precluded the generation of supracritical temperatures and consequent thermally-induced constriction of the vessel wall, providing space for the translocation of blood. The change in reflectance intensity of the perivascular tissue in the irradiated zone (Fig. 6(b), within the dotted line) is likely associated with thermal denaturation of the superficial layers of mesenteric sheath, and namely collagen. Conformational rearrangements associated with collagen denaturation [31] have been reported to occur at temperatures above 40-42˚C [32,33]. The effect is most pronounced at 2000 mW (Fig. 6(b)), mildly enunciated at 1500 mW (Fig. 4(b), arrowheads), and absent at the lowest power settings (Figs. 3(a) and (c)). The graded reflectance profiles at increasing laser powers suggest that the denaturation threshold of the collagenous elements in the mesenteric sheath lies between 1000 and 1500 mW. Moreover, the distance between the hemorrhagic vessel (Fig. 6(b), black arrowhead) and

#5924 - $15.00 US Received 9 December 2004; revised 14 January 2005; accepted 19 January 2005

the constricted vessel (Fig. 6(a), arrowheads) shortened after the laser pulse, probably because of heat-induced shrinkage of collagen [34] and other matrix components.

5. Conclusion

We have introduced a new imaging technique for studying the opto-thermal and hemodynamic responses in laser-irradiated vessels. Although the results are preliminary, the advantages of using DFOPS imaging over conventional microscopic techniques for laser-tissue interaction studies have been clearly demonstrated. The technique is minimally invasive and provides high quality images without the necessity of exogenous contrast agents or fluorophores. Moreover, the high contrast spectral imaging of vascular architecture and individual luminal components enabled the visualization of several laser-tissue interactions that have not been previously reported, although some of these phenomena, such as the laser-induced blood-borne and adherent translucent aggregates, warrant further examination.

Acknowledgments

This work was in part supported by the Technological Collaboration Grant (TSGE 1048) of the Dutch Ministry of Economic Affairs (MH, JFB, MJCvG) and the "Nederlandse Organisatie voor Wetenschappelijk Onderzoek" (NWO) (DJF and MJCvG). The authors would like to thank A. Koeman (Department of Physiology, Academic Medical Center, University of Amsterdam, Amsterdam, The Netherlands) for performing the surgical procedures and providing biotechnical support, Dr. H.S. Tan (Department of Ophthalmology, Academic Medical Center, University of Amsterdam) for making the laser available, G. Huijzer and A. Maas (Department of Experimental Surgery, Academic Medical Center, University of Amsterdam) for provision of blood, L. M. Markvart for the illustration in Fig.1, and Dr. N.J.H. Raat and K.R. Mathura (Department of Physiology, Academic Medical Center, University of Amsterdam) for assistance with video editing. Finally, we thank Professor T.G. van Leeuwen (Laser Center, Academic Medical Center, University of Amsterdam, and Department of Biophysical Engineering, Biomedical Technology Institute, University of Twente, Eschede, The Netherlands) and Dr. P.T. Goedhart (Department of Physiology, Academic Medical Center, University of Amsterdam) for fruitful discussions.

#5924 - $15.00 US Received 9 December 2004; revised 14 January 2005; accepted 19 January 2005